Geological Survey of Japan Cruise Report No. 18, p. 1–35, 1982

PART I

I. THE GH80-1 CRUISE: GENERAL REMARKS

Atsuyuki Mizuno, Seizo Nakao, Masato Joshima,
Osamu Matsubayashi, Yoshihisa Okuda, Koji Onodera,
Takayuki Saito, Katsuya Tsurusaki*, and Akira Usui*

Introduction

This cruise report presents initial scientific results of the R/V Hakurei-Maru GH80–1 cruise (January 12 to March 11, 1980) on two parallel survey lines along the Wake-Tahiti Transect in the Central Pacific Ocean. Part I consists of the results of our shipboard works, and Part II includes the results by our shore-based analyses on sediments and manganese nodules as well as those by non-shipboard scientists.

The cruise was conducted as the first reconaissance phase of the research program of the Geological Survey of Japan (GSJ), *Geological Study of Deep-sea Mineral Resources*, supported by the Agency of Industrial Science and Technology, MITI. It was joined with shipboard works of the research program, *Mining Technology for Marine Mineral Resources*, by the National Research Institute for Pollution and Resources (NRIPR). The research program of GSJ started in 1979 (FY) intending to provide scientific evidences for the origin of manganese nodule deposits through the studies of regional and local variabilities of the deposits and their relation to sedimentary history and geological or geophysical structures in the Wake-Tahiti Transect in the Central Pacific (Fig. I-1).

The transect runs in the NW–SE direction from the east of Wake (17°N) to the west of Tahiti (15°S) across various major geologic provinces, i.e., the southern margin of the Mid-Pacific Mountains, the Central Pacific Basin, the Magellan and Nova-Canton Troughs, the Manihiki Plateau, and the Penrhyn Basin, all of which have been thought to be of early to late Cretaceous origin. General sedimentologic, geologic, and geophysical features of the provinces have been known through the results of DSDP Legs 7, 17, and 33 (WINTERER *et al.*, 1971; WINTERER, EWING *et al.*, 1973; SCHLANGER, JACKSON *et al.*, 1976) and other scientific contributions particularly on geologic structure of some areas (LARSON, 1976; LARSON *et al.*, 1972; ROSENDAHL, 1975; TAMAKI *et al.*, 1979; WINTERER *et al.*, 1974).

Manganese nodule distribution along the transect has been outlined by HORN *et al.* (1972; 1973, for the North Pacific), GLASBY and LAWRENCE (1974, for the South Pacific), and RAWSON and RYAN (1978, for the entire area, with surface sediment lithology). Our research group of the GSJ has delineated the detailed feature of nodule distribution in the northern part of the Central Pacific Basin (MIZUNO and MORITANI, *eds.*, 1977;

*National Research Institute for Pollution and Resources, Tsukuba.

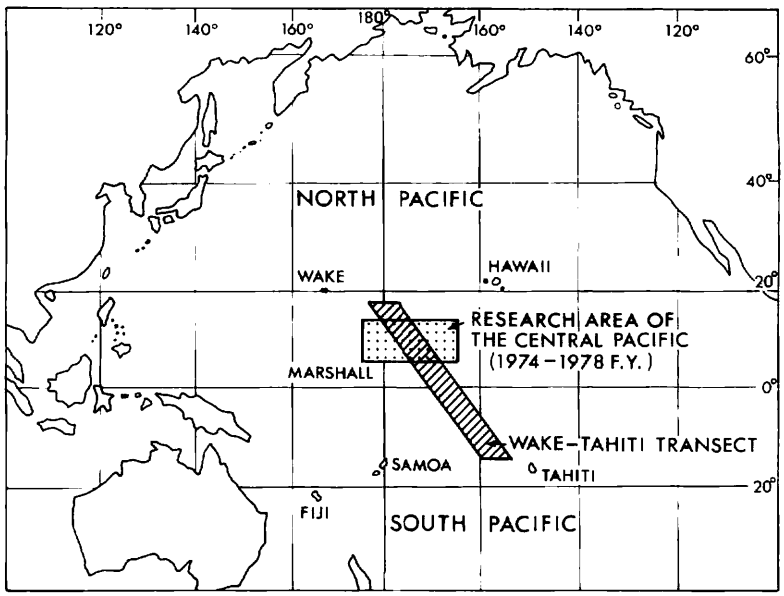

Fig. 1-1 Location of the Wake-Tahiti Transect in the Central Pacific.

MORITANI, *ed.*, 1979; USUI and NAKAO, 1982). According to their data, two distict types of manganese nodule, Type r and Type s, are distributed with varying abundance and metal grade throughout the region, and an additional one, Type b, of which characterization is still not sufficient, sparsely occurs (MIZUNO, 1981). Origin of the diversification of the nodule types has been discussed in relation to Neogene deep-sea sedimentary hiatus and latest Pliocene to Quaternary sedimentary history (MIZUNO, 1981; MIZUNO and MORITANI, 1981). LANDMESSER *et al.* (1976), MONZIER and MISSEGUE (1977), and EXON (1981) reported detailed occurrences of manganese nodules in the Penrhyn Basin on the southern extremity of the transect. The described data suggest that the manganese nodules in the basin have some similarity in nature to the s-type nodules in the Central North Pacific.

The first priority of our study in this cruise was to survey general nodule occurrence and obtain regional data of nodule distribution and its possible relevant factors such as geological, sedimentological, geophysical, and hydrophysical features, throughout the entire transect. For the purpose, our special attention was given to analyse the regional data of nodule, piston cores, box cores, seismic reflection records, bottom water temperature, etc. along two longitudinally parallel survey lines in the transect. Data were also obtained for outlining general geophysical feature of the entire area for reference. Also, we aimed at selecting the areas of detailed study in succeeding phases of the five-year research program which will be particularly devoted for local variability problem of manganese nodule types and properties.

Cruise program and personel

The R/V Hakurei-Maru commanded by Captain Hideaki OKUMURA sailed from Funabashi Port, Tokyo Bay on January 12, 1980 and returned to the port on March 11,

1980, with a port call at Papeete, French Polynesia from February 6 to 13 (Table I-1). We conducted geological and geophysical observations during 32 days along two parallel survey lines within the transect; Line A from 17°N, 177°30′E to 15°S, 158°30′W for the earlier half leg and Line B from 17°N, 180° to 15°S, 156°W for the later half leg, approximately 4,500 km long each. Daily works throughout the cruise are summarized in Appendix I-1.

Shipboard scientific members consisted of the scientists from the Geological Survey of Japan, the National Research Institute for Pollution and Resources, and the Metal

Table I-1 Program of the GH80–1 cruise.

January 12, 1980	Lv. Funabashi (14:00)
	Geophysical survey
January 20	Ar. 17°N, 177°30′E
	Geological and geophysical survey (Line A)
February 4	Lv. West of Tahiti
February 6	Ar. Papeete, Tahiti (08:30)
February 13	Lv. Papeete, Tahiti (16:00)
February 15	Ar. West of Tahiti
	Geological and geophysical survey (Line B)
March 3	Lv. 17°N, 177°30′E
	Geophysical survey
March 11	Ar. Funabashi (09:00)

Table I-2 Shipboard scientific members.

Name	Organization	Speciality and responsibility
Atsuyuki MIZUNO	GSJ	*Chief scientist*; geology, sedimentology, and manganese nodules
Koji ONODERA	*Ibid.*	Bathymetry
Seizo NAKAO	*Ibid.*	Sedimentology
Yoshihisa OKUDA	*Ibid.*	Geology and geophysics
Masato JOSHIMA	*Ibid.*	Geophysics
Osamu MATSUBAYASHI	*Ibid.*	Geophysics
Katsuya TSURUSAKI	NRIPR	Engineering properties of sediments and manganese nodules
Takayuki SAITO	*Ibid.*	*Ibid.*
Yozo BABA*	MMAJ	Survey techniques of manganese nodules
Nobuyuki MASUDA**	*Ibid.*	*Ibid.*
Seijiro OE	Univ. Ryukyus	Undergraduate student; technical assistant
Shoji MISHIMA	*Ibid.*	*Ibid.*
Masahide FURUKAWA	*Ibid.*	*Ibid.*
Yoshikazu MATSUBARA	Kobe Univ.	*Ibid.*
Shinichi YOSHIMI	*Ibid.*	*Ibid.*
Yasuhiro KAWAKAMI	Kyoto Univ.	Graduate student; technical assistant
Mikio MITAMURA	Chiba Univ.	*Ibid.*
Ikuhisa ADACHI	*Ibid.*	Undergraduate student; technical assistant
Akira USUI	Univ. Tokyo	Graduate student; manganese nodules (presently GSJ scientist)
Anthony UTANGA*	Govt. Cook Islands	Survey techniques of manganese nodules
Faataia MALELE**	Govt. West Samoa	*Ibid.*

*Funabashi to Papeete.
**Papeete to Funabashi.

Mining Agency of Japan (MMAJ). Graduate and undergraduate students from some universities participated in the cruise as technical assistants (Table I-2).

Two trainees from CCOP-SOPAC member countries, funded by ESCAP, also participated in the cruise and collaborated with us to learn shipboard survey techniques; A. UTANGA from the Government of Cook Islands in the earlier half leg and F. MALELE from the Government of West Samoa in the later half leg.

Shipboard observations

We used NNSS instrumentation for positioning throughout the entire cruise. The real time positions obtained were recalculated based on estimated water current to make the accuracy as high as possible. The estimated errors ranged from 190 m (0.1 n.m.) to 740 m (0.4 n.m.) in the worst case, as shown in Appendix I-2. Some problems concerning the positioning were discussed elsewhere (JOSHIMA, 1980).

Geological and geophysical observations on the two survey lines comprised echo-sounding, continuous seismic reflection profiler survey by air-gun, seismic refraction survey by sono radiobuoy, geomagnetic survey, gravimetric survey, heat flow measurement, sampling of sediment and manganese nodule by box corer, piston corer, and freefall grab, and bottom-photographing by freefall camera attached to freefall grab and deep-sea camera attached to the box corer. Sediment and nodule samples were visually and microscopically observed, measured, and/or analysed in the shipboard laboratories (Table I-3).

Table I-3 Observation method along Lines A and B.
The right-hand column shows a survey line length and an observation number of respective work.
Total cruise distance: 21,663 km
Length of Lines A and B: 4,500 km each
Cruising and positioning: by NNSS
Line A: 17°N, 177°30'E to 15°S, 158°30'W
Line B: 17°N, 180° to 15°S, 156°W

Bathymetric survey by 12 kHz PDR	9,000 km
Subbottom profiling by 3.5 kHz PDR	9,000 km
Continuous seismic reflection survey by air-gun	9,000 km
Seismic refraction survey by sono radio-buoy	3 sites
Magnetic survey by proton magnetometer	9,000 km
Gravimetric survey by onboard gravimeter	9,000 km
Heat flow measurement (associated with sampling by piston corer)	21 stations (H15–35)
Bottom sampling by box corer	32 stations (B1–32)
Bottom sampling and photographing by freefall grab and camera	61 stations (FG191–251)
Bottom sampling by piston corer	22 stations (P158–179)
Bottom sampling by large box dredge	2 stations (D377–378)
In-situ measurement of substrate physical properties	1 stations (FV2)
On board examinations on sediments and nodules	
Sediments: visual description, smear slide observation, coarse fraction analysis by sedimentation tube, soft X-ray radiography, and measurements of water content and shear strength.	
manganese nodules: visual description, morphologic classification, measurement of size and weight, and polishing and description of cut surface.	

Sampling and bottom-photographing stations (Sts. 1589 to 1647) were arranged basically at intervals of 110 km and 190 km on the two survey lines. Box-core sampling and piston-core sampling were conducted alternately in principle at the stations except for those on the northern half of Line A (Fig. I-2, Table I-4). At all the stations two sets of freefall grab installing a camera were used for additional sampling and photographing. Works only by the freefall grab and camera were conducted at some stations on Line A.

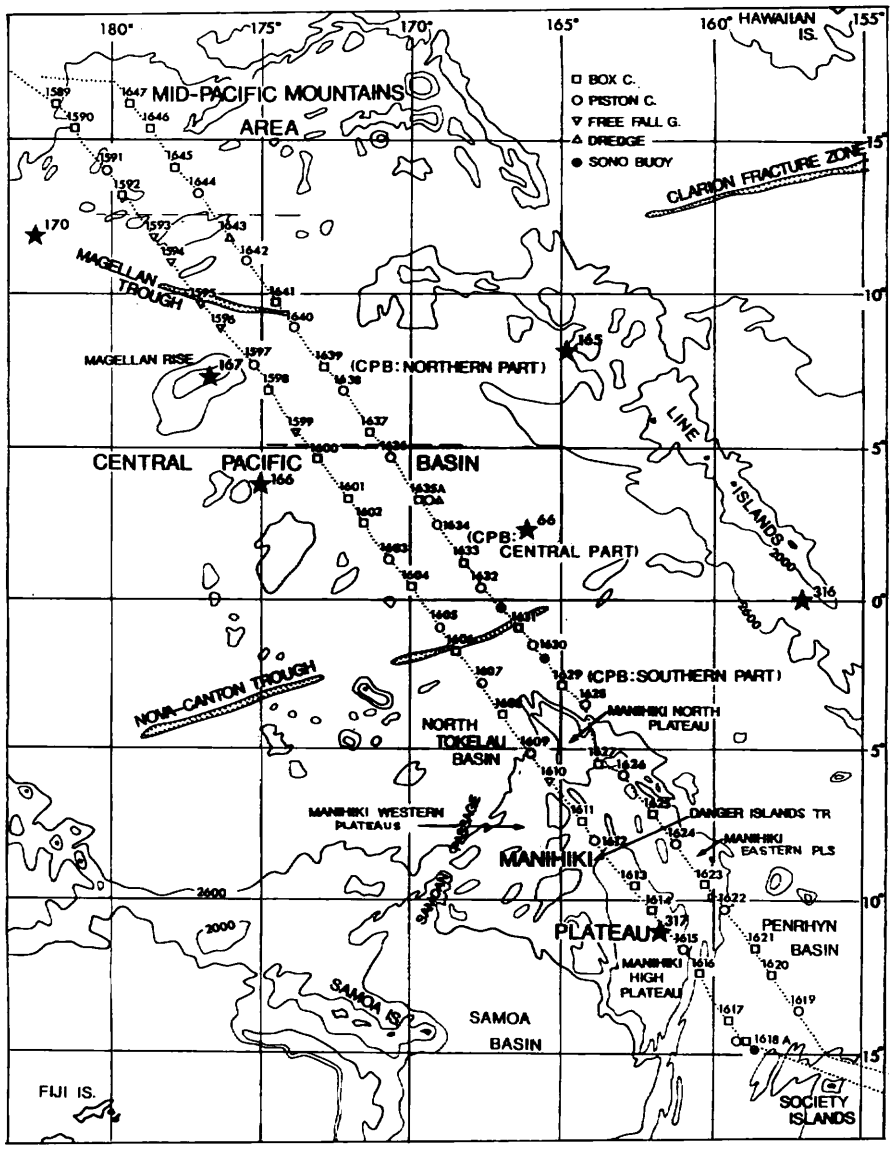

Fig. I-2 Sampling and bottom-photographing stations on Lines A (1589 to 1618A) and B (1619 to 1647) with divisions of topographic province. Bathymetric contours (in fathom) are based on CHASE *et al.* (1971) and MAMMERICKX *et al.* (1975).

Table I-4 Representative position and water depth of each station, GH80-1 cruise.

Line A				Topographic province	Line B			
St. No.	W. D. (m)	Position			St. No.	W. D. (m)	Position	
1589(B)	4580	16°12'N	178°10'E	Mid-Pacific Mountains area	1647(B)	5290	16°10'N	179°20'W
1590(B)	5300	15°24'N	178°44'E		1646(B)	5520	15°23'N	178°45'W
1591(P)	5560	14°03'N	179°45'E		1645(B)	5100	14°06'N	177°47'W
1592(B)	5600	13°15'N	179°38'W		1644(P)	5030	13°17'N	177°08'W
1593(FG)	5500	11°54'N	178°36'W	CPB: Magellan Trough northern part	1643(B)	5260	11°49'N	176°06'W
1594(FG)	5800	11°05'N	177°58'W		1642(P)	5430	11°06'N	175°29'W
1595(FG)	6200	09°46'N	176°58'W		1641(B)	5830	09°47'N	174°31'W
1596(FG)	6100	08°56'N	176°23'W		1640(P)	5910	08°58'N	173°53'W
1597(FG)	5940	07°38'N	175°14'W		1639(B)	5910	07°40'N	172°56'W
1598(B)	5960	06°50'N	174°48'W		1638(P)	5800	06°49'N	172°15'W
1599(FG)	5200	05°27'N	173°46'W		1637(B)	5970	05°31'N	171°19'W
1600(B)	5590	04°41'N	173°12'W	CPB: central part Nova-Canton Trough CPB: southern part NTB MWP DIT MHP Manihiki Plateau Manihiki E Pl	1636(P)	5740	04°43'N	170°42'W
1601(B)	5340	03°17'N	172°10'W		1635(BPD)	5350	03°16'N	169°41'W
1602(B)	5390	02°33'N	171°37'W		1634(P)	5080	02°32'N	169°06'W
1603(P)	5500	01°17'N	170°42'W		1633(B)	5080	01°16'N	168°10'W
1604(B)	5460	00°25'N	170°03'W		1632(P)	5250	00°26'N	167°34'W
1605(P)	5460	00°58'S	169°02'W		1631(B)	5350	00°59'S	166°20'W
1606(B)	5220	01°45'S	168°26'W		1630(P)	5500	01°31'S	165°52'W
1607(P)	5690	03°02'S	167°29'W		1629(B)	5210	02°53'S	164°57'W
1608(B)	5500	03°52'S	166°52'W		1628(P)	4980	03°31'S	164°10'W
1609(P)	4400	05°12'S	165°51'W		1627(B)	5000	05°27'S	163°46'W
1610(FG)	2800	06°02'S	165°22'W		1626(P)	4710	05°47'S	162°56'W
1611(B)	4160	07°21'S	164°17'W		1625(B)	4650	07°07'S	161°56'W
1612(P)	4810	08°20'S	163°48'W		1624(P)	3900	08°08'S	161°12'W
1613(B)	2950	09°29'S	162°41'W		1623(B)	4550	09°26'S	160°15'W
1614(B)	2760	10°16'S	162°05'W		1622(P)	5230	10°16'S	159°35'W
1615(P)	3160	11°36'S	161°05'W		1621(B)	5310	11°35'S	158°35'W
1616(B)	5650	12°20'S	160°31'W	Penrhyn Basin	1620(B)	5270	12°26'S	157°57'W
1617(B)	5150	13°47'S	159°28'W		1619(BP)	5100	13°34'S	157°05'W
1618(BP)	5500	14°29'S	158°53'W		——	——	——	——

Heat flow measurement was done with a thermograd-meter attached to a piston corer. The thermograd-meter also measured temperature of near-bottom sea water.

The stations were connected with underway observations under a ship speed of 10 knots, which comprised 12 kHz echo-sounding, 3.5 kHz subbottom profiling, continuous seismic profiling survey, geomagnetic survey, and gravimetric survey (Fig. I-3). Depth data obtained by a 12 kHz PDR were corrected for velocity of sound in seawater by MATTHEW's table. Seismic refraction survey was conducted at three selected places in the Penrhyn Basin and the vicinity of the Nova-Canton Trough, but unfortunately we could obtain no effective result to discuss the nature of crustal structure.

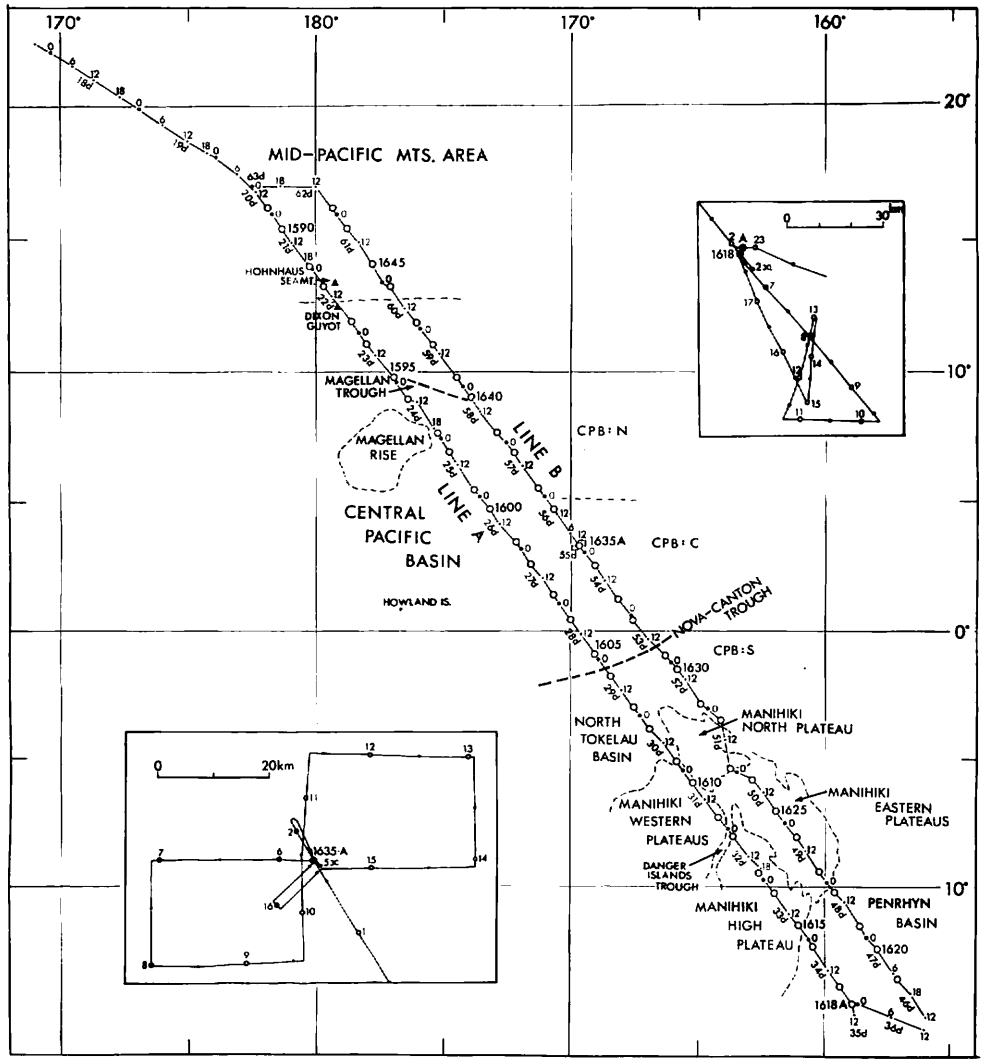

Fig. I-3 Location of the two survey lines, with positions of the mid-night and the noon of each day (UT). Additional tracks near Sts. 1635A and 1618A are enlarged separately within this figure.

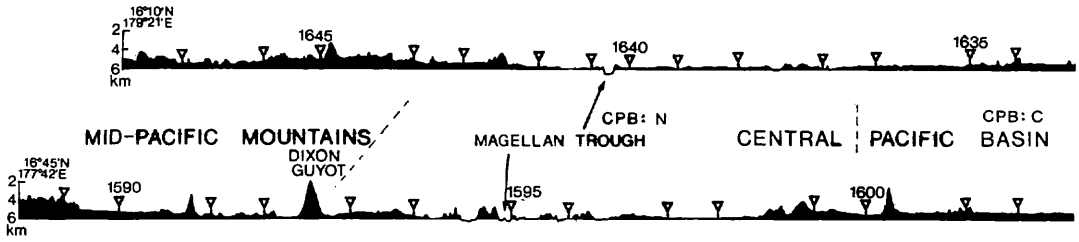

Fig. I-4 Bathymetric profiles of Lines A and B, drawn by an

Topographic provinces, bathymetric profiles, and local bathymetric maps

For convenience of description, we here define and name the topographic provinces along the transect as shown in Fig. I-2 and Table I-4, largely following to conventional use and partly to WINTERER *et al.* (1974) (Manihiki Plateau region). The province, *Manihiki Eastern Plateaus*, is newly named to the northeastern area of the Manihiki Plateau region. It is located on the southeast of the Manihiki North Plateau and on the northeast of the Manihiki High Plateau, and is characterized by a wide development of rough topography deeper than those but shallower than the Central Pacific Basin and the Penrhyn Basin (less than 5 km deep). The wide Central Pacific Basin is divided into three, northern, central, and southern parts, arbitrarily.

Figure I-4 presents bathymetric profiles of the two survey lines with an indication of sampling and bottom-photographing stations, based on our results of echo-sounding. Bathymetric feature of each topographic province on the profiles will be described in Chap. III. Based on the data of corrected water depth and recalculated positions we completed a detailed local bathymetric map of each station area to provide a basis particularly for consideration of local variation of manganese nodules. The maps are incorporated into the figures in Appendix VII-1 (Chap. VII).

Field data of on-site observations

Field data of our on-site observations are summarized in Appendix I-2. It includes the data of recalculated position, its accuracy, corrected water depth, lithology of surface sediment, morphologic types and abundance and/or coverage of manganese nodules, topographic and acoustic properties, and summarized lithologic sequence of piston core, at each station areas. Usually observations by means of different instruments were separately conducted, and respective data excluding topographic and acoustic properties are described for each observation sites.

Geophysical and geological data

Two magnetic anomaly lineation sets, the Magellan lineations and the Phoenix lineations were evidently detected along Lines A and B in the northern to central Central Pacific Basin. Magnetic anomaly lineations on both, northern and southern sides of the Nova-Canton Trough are indistinct. Those in the Penrhyn Basin are characterized by small amplitude and short wave length, suggestive of origin of the basin during the late Cretaceous magnetic quiet zone (Chap. II).

Free-air gravity anomaly is generally -10 to -20 mgal in deep-sea basin areas,

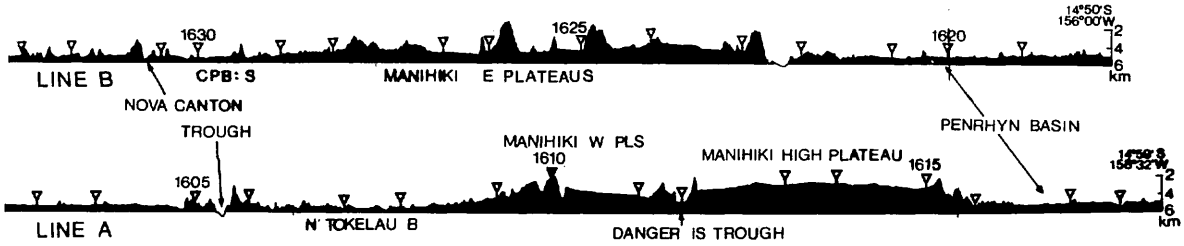

auto-plotter on R/V Hakurei-Maru, based on 12 kHz records.

whereas it ranges from +50 to +100 mgal in seamount and plateau areas (Chap. II).

Crustal heat flow value measured by a thermograd-meter averages 53.9 ± 13.1 mW m^{-2} (1.29 ± 0.31 HFU) on highly reliable data from seven sites on the two traverses, ranging from 34.9 to 69.0 mW m^{-2} (0.83 to 1.65 HFU). The obtained values are thought to be of normal for the Central Pacific Ocean, and anomalously higher or lower value of heat flow was not detected (Chap. IV).

We measured a sea water temperature (T *in situ*) in the lowest water column (from 7.5 m to about 1,000 m above the sea bottom) by the thermograd-meter (Chap. IX), and calculated a potential temperature (Tp) of the near-bottom water. Two types of vertical profile of T *in situ* can be recognized along the traverses. One is characterized by nearly adiabatic temperature profile having a minimum temperature at depths of 4,500 to 5,150 m and is commonly found at the stations mostly deeper than 5,600 m in the Central Pacific Basin. Another has no temperature minimum and is characterized by monotonically decreasing curve from upper to lower waters. Vertical distribution of T *in situ* on and around the Manihiki Plateau suggests that heat flow from the earth is laterally removed by flowing water more effectively than the cases of the first type which has adiabatic temperature profile of the bottom water. Tp values of the near-bottom water indicate a possible clockwise turn of the PBW which is originated from the AABW and passed through the Samoan Passage into the North Tokelau Basin, and also suggest a very slow northerly movement of bottom water in the northern and central Central Pacific Basin.

Seismic reflection survey revealed that sediment sequence on aoustic basements is divided into Unit I and Unit II in most areas of deep-sea basin, excluding the Manihiki Plateau region. Unit II consists mainly of opaque layer and tends to thin southward from 0.40 to 0.05 sec thick., having nearly identical acoustic facies in deep-sea basin. In many places Unit II is separated from overlying Unit I by a strong reflector possibly of cherty chalk or chert of middle Eocene to Oligocene. Unit I is characterized by regionally varying thickness and acoustic facies. It is represented by thick transparent acoustic nature in deep-sea basins of the middle region of the transect, given by fast accumulation of siliceous sediments; whereas by thinner transparent layer, occasionally replaced by reflective layers, or is missing in the northern and southern regions, contributed by slow accumulation of pelagic clay. In some places near large seamount, ridge, and plateau, Unit I or Unit I-II is represented by turbidites origin coherent acoustic nature. On shallower bottom of the Manihiki High Plateau and parts of the Manihiki Western and Eastern Plateaus, there has been accumulation of calcareous ooze/chalk during the late

Eocene to Quaternary, which is represented by transparent or subtransparent acoustic facies with weak stratification. A middle-late Eocene hiatus appears to be rather widely distributed in the northern and central regions in the northern hemisphere and also in some parts of the Manihiki Plateau region (Chap. III).

Sedimentological data

Based on the surface sediment lithology, the transect area can be divided into the following sedimentary provinces; northern pelagic clay zone, transitional zone, equatorial siliceous biogenic zone, equatorial calcareous biogenic zone, and southern pelagic zone, from north to south. Piston core lithology, micropaleontology (Chapters X and XI), and remanent magnetization (Chap. XII) indicate that sedimentation during the mid-Tertiary through the Quaternary has been controlled by almost identical aspects of bathymetry, biologic productivity, volcanism, supply of terrigenous materials, etc. in respective provinces, except for the transitional zone. Sedimentary structures suggestive of resedimentation or redistribution processes in the past are found in cores from seamount and plateau areas and their vicinity. Deep-sea hiatuses and very shortened interval of the entire Quaternary or the late Pleistocene to Recent occur extensively through the two traverses (Chap. V).

Clay minerals in fraction under 2 μm of surface sediments and piston cores are represented by montmorillonite, illite, chlorite, and kaolinite (in order of abundance), which show no particular pattern of regional distribution. Clinoptilolite was detected in part of cores from the Mid-Pacific Mountains area and the Penrhyn Basin (Chap. XIII).

Major element and minor element chemistry of the sediments show some noticeable aspects (Chapters XIV and XV, respectively). $CaCO_3$ is contained in considerable amount in core sediments within 60 cm from the top, which were obtained from the depths below CCD. Concentrations of MnO, Fe_2O_3, and P_2O_5 are generally higher than the sediments from the GH79–1 area, suggesting slower sedimentation rate and/or higher biological activity. Major element chemistry shows that the sediments on the Manihiki Plateau have been partly contributed by the Tahiti-type volcanic activity possibly on the plateau. Concentration of Mn in surface sediments varies with their lithology. It amounts to 0.5% or more in pelagic clay and zeolitic mud, and exceeds 2% in some sites of the Penrhyn Basin. Fe, Co, Ni, and Pb show the similar tendency of distribution in general, and are in strong positive correlation with each other, together with Mn, suggesting at least common ultimate source of these elements. Examination of black magnetic spherules in the sediments resulted in that Ir/Fe, Au/Fe, and Co/Fe in those larger than 400 μm tend to decrease with increasing particle size (Chap. XIX).

Geotechnical properties of the surface and core sediments are generally related to sediment lithology. In cores consisting of monotonous lithology water content decreases and vane shear strength increases with a depth of burial. In cores including various lithologic types or turbidites the geotechnical properties change irregularly with lithologic change. Averaged adhesiveness between manganese nodule and surface sediments was measured 5.8 ± 1.9 gr/cm^2 (per nodule projection area) (Chap. VI).

Data on manganese nodules

Based on manganese nodule samples collected by a box corer, a freefall grab, or a piston corer, and bottom photographs, the following studies have been conducted: distribution of nodule types and their geological occurrences (Chap. VII), mineralogy by X-ray diffraction analysis (Chap. XVII), geochemistry by atomic absorption spectroscopic analysis (for Mn, Fe, Cu, Ni, Co, Pb, and Zn) (Chap. XVI), micronodules (Chap. XVIII), and estimation of nodule abundance from nodule coverage measured on bottom photographs (Chap. VIII).

Manganese nodules throughout the transect area can be divided into three morphologic types from the viewpoints of morphology (including surface texture), occurrence, abundance, chemistry, mineralogy, and internal structure. They are: (1) s-type nodules in the Mid-Pacific Mountains area and the Central Pacific Basin, (2) r-type nodules in the Central Pacific Basin, and (3) s-type nodules in the Penrhyn Basin. The Manihiki Plateau and its environs where calcareous ooze dominantly occurs are generally barren or poor in manganese nodule. Types (1) and (3) are commonly characterized by their occurrence in pelagic clay and zeolitic mud, exposing to bottom water, having smooth surface, high abundance (more than 10 kg/m^2), and low Mn/Fe ration and Cu plus Ni grade (1.4 to 1.3 and 0.85% on the average, respectively). However, Type (3) has a simple internal structure consisting largely of δ-MnO_2 phase, whereas Type (1) has a double internal structure which consists of internal part of δ-MnO_2 phase and outer layer of δ-MnO_2 phase and 10 Å manganite phase. Type (2) occurs in siliceous clay or ooze, being burried in the sediments, and is characterized by rough surface, higher Mn/Fe ratio and Cu plus Ni grade (4.1 and 2.41% on the average, respectively), and lower abundance (less than 10 kg/m^2). The morphology, occurrence, and chemical property have been likely controlled by selective formation and growth of the two mineral phases.

The three types of manganese nodules are evidently related to regional variation of sediment lithology and have been caused by various factors of sedimentation, particularly of biogenetic, sedimentary rate, activity of bottom current, volcanism, etc. during the mid-Tertiary (?) through the Quaternary. From regional data of nodule distribution, Type (2) (=r-type nodules in the Central Pacific Basin) has formed under the environment of siliceous ooze and siliceous clay sedimentation through the Pliocene and the Quaternary in some cases interrupted by deep-sea hiatus, and Types (1) and (3) (=s-type nodules in the Mid-Pacific Mountains and the Penrhyn Basin, respectively) has formed under non-depositional environment at least during the late Pleistocene to Holocene, associated with pelagic clay or zeolitic mud of the pre-Pleistocene or the pre-late Pleistocene.

Local variation of distribution of the types was detected in some station areas. Its detailed feature and the origin of difference of Types (1) and (3) remain to be strudied through investigations in the succeeding years.

References

CHASE, T. E., MENARD, H. W. W., and MAMMERICKX, J. (1971) *Topography of the North Pacific. IMR Tech. Rept. Ser.* TR 14.

EXON, N. F. (1981) Manganese nodules in the Cook Islands region, Southwest Pacific. *South Pac. Mar. Geol. Notes,* vol. 2, p. 47–65.

GLASBY, G. P. and LAWRENCE, P. (1974) *Manganese Deposits in the South Pacific Ocean* (scale 1 : 25000000). *N. Z. Oceanogr. Inst. Chart, Misc. Ser.*, 33–38.

HORN, D. R., DELACH, M. N., and HORN, B. M. (1973) Metal content of ferromanganese deposits of the Oceans. *Tech. Rept.*, no. 3, NSF GX-33616, Office IDOE, NSF, Washington, D. C., p. 1–51.

————, HORN, B. M., and DELACH, M. N. (1972) Ferromanganese deposits of the North Pacific. *Tech. Rept.*, no. 1, NSF GX-33616, Office, IDOE, NSF, Washington, D. C., p. 1–78.

JOSHIMA, M. (1980) On the positioning by NNSS. *In* MIZUNO, A. *et al.*, Geological studies on the deep-sea mineral resources, Hakurei-Maru GH80–1 cruise, *Chishitsu News*, no. 316, p. 41–45 (in Japanese).

LANDMESSER, C. W., KROENKE, L. W., GLASBY, G. P., SAWTEL, G. H., KINGAN, S., UTANGA, E., UTANGA, A., and COWAN, G. C. (1976) Manganese nodules from the South Penrhyn Basin, Southwest Pacific. *South Pac. Mar. Geol. Notes*, vol. 1, p. 17–39.

LARSON, R. L. (1976) Late Jurassic and early Cretaceous evolution of the western Central Pacific Ocean. *Jour. Geomag. Geoelectr.*, vol. 28, p. 219–236.

————, SMITH, S. M., and CHASE, C. G. (1972) Magnetic lineations of early Cretaceous age in the western equatorial Pacific Ocean. *Earth Planet. Sci. Lett.*, vol. 15, p. 315–319.

MAMMERICKX, J., SMITH, S. M., TAYLOR, I. L., and CHASE, T. E. (1975) *Topography of the South Pacific. IMR Tech. Rept. Ser.* TR 56.

MIZUNO, A. (1981) Regional and local variabilities of manganese nodules in the Central Pacific Basin. *In* MIZUNO, A. (*ed.*), *Geol. Surv. Japan Cruise Rept.*, no. 15, p. 281–296.

———— and MORITANI, T. (*eds.*) (1977) Deep sea mineral resources investigation in the central-eastern part of Central Pacific Basin, January-March, 1976 (GH76–1 cruise). *Geol. Surv. Japan Cruise Rept.*, no. 8, p. 1–217.

———— and ———— (1981) Deep-sea manganese nodules and sedimentary hiatuses. *Marine Sciences*, vol. 13, p. 122–125; p. 180–190 (in Japanese).

MONZIER, M. and MISSEGUE, F. (1977) Prelevement de nodules polymetalliques dans l'Archipel de Cook, Missions "Danaides 2" et "Geotransit 2". Rapport preliminaire. ORSTOM-CNEXO.

MORITANI, T. (*ed.*) (1979) Deep sea mineral resources investigation in the central-western part of Central Pacific Basin, January-March 1977 (GH77–1 cruise). *Geol. Surv. Japan Cruise Rept.*, no. 12, p. 1–256.

RAWSON, M. D. and RYAN, W. B. F. (1978) *Ocean Floor Sediments and Polymetallic Nodules*. Lamont-Doherty Geological Observatory, Columbia Univ., Palisades, N. Y.

ROSENDAHL, B. R. (1975) Geological and geophysical studies of the Canton Trough region. *Jour. Geophys. Res.*, vol. 80, p. 2565–2574.

SCHLANGER, S. O., JACKSON, E. D., *et al.* (1976) *Initial Reports of the Deep Sea Drilling Project*, vol. 33, Washington, U. S. Govt. Printing Office, p. i-xx, 1–973.

TAMAKI, K., JOSHIMA, M., and LARSON, R. L. (1979) Remanent early Cretaceous spreading center in the Central Pacific Basin. *Jour. Geophys. Res.*, vol. 84, p.

4501–4510.

USUI, A. and NAKAO, S. (1982) *Manganese Nodule Distribution in the Central Pacific Ocean. Geol. Surv. Japan Mar. Geol. Map. Ser.* (in preparation).

WINTERER, E. L. *et al.* (1971) *Initial Report of the Deep Sea Drilling Project*, vol. 7, Washington, U. S. Govt. Printing Office, p. i-xix, 1–1757.

————, EWING, J. I., *et al.* (1973) *Initial Reports of the Deep Sea Drilling Project*, vol. 17, Washington, U. S. Govt. Printing Office, p. i-xx, 1–930.

————, LONSDALE, P. F., MATTHEWS, J. L., and ROSENDAHL, B. R. (1974) Bathymetry, structure and acoustic stratigraphy of the Manihiki Plateau. *Deep-Sea Res.*, vol. 21, p. 793–814.

Appendix I-1 Daily works of the GH80–1 cruise.

Date	Weather	Cruising time	Cruising distance (n.m.)	Works on board		
				On-site observation	Underway observation	
January						
12	Fine	09.30	129.8	Lv. Funabashi (14:00)	G 12 3.5	
13	Cloudy	23.30	303.4		G M 12 3.5	
14	Fine	23.30	297.2		G M 12 3.5	
15	Fine	23.30	336.1		G M 12 3.5	
16	Fine	23.30	334.0		G M 12 3.5	
17	Cloudy/ Fine	23.30	292.9		G M A 12 3.5	
18	Fine	24.00	246.5		G M A 12 3.5	
19	Fine	24.00	244.9		G M A 12 3.5	
20	Fine	24.00	197.3	Ar. 17°00′N, 177°30′E(22:02)	G M A 12 3.5	
21	Fine	24.00	150.6	1589 (B(s)1, FG191–1, 2) 1590 (B(s)2, FG192–1, 2)	G M A 12 3.5	
22	Fine	24.00	166.1	1591 (P158, FG193–1, 2) 1592 (B(s)3, FG194–1, 2)	G M A 12 3.5	
22	Cloudy	24.00	203.0	1593 (FG195–1, 2) 1594 (FG196–1～5)	G M A 12 3.5	
23	Cloudy	24.00	188.9	1595 (FG197–1～4) 1596 (FG198–1～4)	G M A 12 3.5	
24	Cloudy	24.00	177.7	1597 (FG199–1, 2) 1598 (B4, FG200–1, 2)	G M A 12 3.5	
25	Fine	24.00	193.1	1599 (FG201–1～5) 1600 (B5, FG202–1, 2)	G M A 12 3.5	
26	Fine	24.00	169.4	1601 (B6, FG203–1, 2) 1602 (B7, FG204–1, 2)	G M A 12 3.5	
27	Fine	24.00	175.8	1603 (P159, FG205–1, 2, H15) 1604 (B8, FG206–1, 2)	G M A 12 3.5	
28	Fine	24.00	176.4	1605 (P160, FG207–1, 2, H16) 1606 (B9, FG208–1, 2)	G M A 12 3.5 passing the Equator (22:40)	
29	Fine	24.00	169.2	1607 (P161, FG209–1, 2, H17) 1608 (B10, FG210–1, 2)	G M A 12 3.5	
30	Fine	24.00	196.8	1609 (P162, FG211–1, 2, H18) 1610 (FG212–1～4)	G M A 12 3.5	
31	Fine	24.00	188.4	1611 (B11, FG213–1, 2) 1612 (P163, FG214–1, 2, H19)	G M A 12 3.5	
February						
1	Fine	24.00	213.1	1613 (B12, FG215–1, 2) 1614 (B(s)13, FG216–1, 2)	G M A 12 3.5	
2	Cloudy	24.00	188.8	1615 (P164, FG217–1, 2, H20) 1616 (B14, FG218–1, 2)	G M A 12 3.5	
3	Rainy/ Cloudy	24.00	191.4	1617 (B15, FG219–1, 2) 1618 (B16, FG220–1, 2)	G M A 12 3.5	
4	Rainy/ Cloudy	23.30	248.0	1618A (P165, FG221–1, 2, H21, FV2)	G M A 12 3.5	S
5	Cloudy	23.30	330.7			
6	Cloudy	08.30	75.2	Ar. Papeete (08:30)		
7	Cloudy					
8	Cloudy					
9	Cloudy					
10	Cloudy					
11	Cloudy					
12	Rainy					
13	Cloudy	08.30	68.4	Lv. Papeete (16:00)		

Appendix I-1 (Continued)

Date	Weather	Cruising time	Cruising distance (n.m.)	Works on board						
				On-site observation	Underway observation					
14	Fine	24.30	330.5							
15	Fine	24.00	195.1	1619 (P166, FG222–1, 2, H22, B17)	G	M	A	12	3.5	
16	Fine	24.00	194.0	1620 (B18, FG223–1, 2) 1621 (B19, FG224–1, 2)	G	M	A	12	3.5	
17	Fine	24.00	178.2	1622 (P167, FG225–1, 2, H23) 1623 (B20, FG226–1, 2)	G	M	A	12	3.5	
18	Fine	24.00	192.1	1624 (P168, FG227–1, 2, H24) 1625 (B21, FG228–1, 2)	G	M	A	12	3.5	
19	Fine	24.00	195.1	1626 (P169, FG229–1, 2, H25) 1627 (B22, FG230–1, 2)	G	M	A	12	3.5	
20	Fine	24.00	193.8	1628 (P170, FG231–1, 2, H26) 1629 (B23, FG232–1, 2)	G	M	A	12	3.5	
21	Fine	24.00	186.3	1630 (P171, FG233–1, 2, H27) 1631 (B24, FG234–1, 2)	G	M	A	12	3.5	S
22	Fine	24.00	195.0	1632 (P172, FG235–1, 2, H28) 1633 (B25, FG236–1, 2)	G	M	A	12	3.5	S
					passing the Equator (05:40)					
23	Fine	24.00	195.6	1634 (P173, FG237–1, 2, H29) 1635 (B26, FG238–1, 2)	G	M	A	12	3.5	
24	Fine	24.00	155.9	1635A (P174, FG239–1, 2, H30, D377, test of deep-tow magnetometer)	G	M	A	12	3.5	
25	Fine	24.00	182.7	1636 (P175, FG240–1, 2, H31) 1637 (B27, FG241–1, 2)	G	M	A	12	3.5	
26	Fine	24.00	182.4	1638 (P176, FG242–1, 2, H32) 1639 (B28, FG243–1, 2)	G	M	A	12	3.5	
27	Fine	24.00	180.6	1640 (P177, FG244–1, 2, H33) 1641 (B29, FG245–1, 2)	G	M	A	12	3.5	
28	Fine	24.00	169.3	1642 (P178, FG246–1, 2, H34) 1643 (D378, FG247–1, 2)	G	M	A	12	3.5	
29	Fine	24.00	196.6	1644 (P179, FG248–1, 2, H35) 1645 (B30, FG249–1, 2)	G	M	A	12	3.5	
March										
1	Fine	24.30	196.4	1646 (B31, FG250–1, 2) 1647 (B32, FG251–1, 2)	G	M	A	12	3.5	
3	Fine	24.30	291.4	Lv. 17°00′N, 177°30′E(13:00)	G	M	A	3.5		
4	Fine	24.30	333.8		G	M	3.5			
5	Fine	24.30	332.9		G	M	3.5			
6	Fine	24.30	333.9		G	M	3.5			
7	Cloudy	24.30	337.6		G	M	3.5			
8	Cloudy	24.30	306.7		G	M	3.5			
9	Cloudy	24.30	282.1		G	M	3.5			
10	Cloudy	24.00	282.7		G	M	3.5			
11	Cloudy	02.15	23.4		G					

Total distance 11697.2 (n.m.) (21663 km)

Total cruising time 1229 h 15 min.

Abbreviations:

B (double spade box corer), B(s) (single spade box corer) 1～32; P (piston corer, GH 80–1 type) 158～179, associated with H (heat flow meter, GH80–1 type) 15～37; FG (freefall grab) 191～251; D (large box dredge) 377～378; FV (freefall vanetester) 2. NS (NNSS); G (gravity meter); M (proton magnetometer); A (air-gun); S (sono-buoy); 12 (12 kHz PDR); 3.5 (3.5 kHz PDR).

Appendix I-2 Results of on-site

St. no.	Observ. no.	Date		Recalculated position			Corrected depth (m)
		Julian	Local	Latitude	Longitude	E.E.*	
		January	January				
1589	B(s)1(c)	20	21	16°11.38′N	178°09.27′E	0.22	4378
	FG191–1			16°11.74′N	178°09.94′E	0.23	4588
	FG191–2(c)			16°11.85′N	178°10.07′E	0.24	4594
1590	B(s)2	21	21	15°23.31′N	178°43.79′E	0.13	5287
	FG192–1(c)			15°23.67′N	178°44.00′E	0.17	5306
	FG192–2(c)			15°23.61′N	178°44.01′E	0.16	5306
1591	P158	21	22(1)	14°02.91′N	179°44.90′E	0.14	5550
	FG193–1(c)			14°03.09′N	179°45.80′E	0.20	5569
	FG193–2(c)			14°02.97′N	179°45.83′E	0.21	5571
1592	B3	22	22(1)	Unsuccessful			
	FG194–1(c)			13°14.65′N	179°37.55′W	0.24	5596
	FG194–2(c)			13°14.56′N	179°37.51′W	0.25	5596
1593	FG195–1	22	22(2)	11°54.16′N	178°36.28′W	0.21	5491
	FG195–2(c)			11°54.06′N	178°36.24′W	0.22	5489
1594	FG196–1(c)	23	22(2)	11°06.91′N	178°00.01′W	0.41	5729
	FG196–2			11°06.19′N	177°59.45′W	0.38	5736
	FG196–3(c)			11°05.47′N	177°58.45′W	0.35	5814
	FG196–4(c)			11°04.77′N	177°58.20′W	0.32	5870
	FG196–5(c)			11°04.03′N	177°57.59′W	0.29	5886

*Estimated error (in n.m.).

observations, GH80–1 Cruise.

Bottom sediment**	Manganese nodules			Topography and others***
	Morphology	Abun. (kg/m²)	Cover. (%)	
No sediment. Fragment of manganese crust	(DPs)	(13g)	60	very rough, without a transparent layer on both seismic reflection and 3.5 kHz records. Sediment veneer appears to cover the basement of basalt.
Brown to dark brown zeolite-rich clay basalt fragments	No sample	0	—	
Brown to dark brown zeolite-rich clay basalt fragments	No sample	0	30	
Dark yellowish brown zeolite-rich clay	DPs+r, IDPs+r	6.2	—	Smooth; very thin 3.5 kHz transparent layer locally developed; seismic reflection transparent layer is not recognized.
Dark yellowish brown zeolitic mud	Ds, IDPs	5.5	40	
Dark yellowish brown zeolitic mud	Ds, Ss	1.1	25	
Dark brown zeolitic clay (top of pilot core)	No sample	0	—	Rolled; 3.5 kHz transparent layer several meters thick; no seismic reflection transparent layer. P158 (2.01 m long) largely consists of dark brown (upper half) to very dusky red (lower half) zeolitic clay (zeolite up to 40%).
Dark brown zeolite-rich clay	Sr	0.1	1	
Dark brown zeolite-rich clay	Sr, SEr	0.1	2	
Brown to dark brown clay	DPs·r, IDs·r	1.5	— 5	Rolled; the sampling sites are on topographically high area; 3.5 kHz transparent layer is very thin to absent; no seismic reflection data.
Brown to dark brown clay	DPs·r, Ss·r	0.9	8	
Dark brown clay	Ds·r, Ss·r	1.3	—	Smooth; 3.5 kHz transparent layer approximately 10 m thick; no seismic reflection transparent layer.
Dark brown clay	IDPs+r, Ss·r	0.9	10	
Brown to dark brown clay	IDPs, DPs	16.1	80	Sloped and slightly rolled; 3.5 kHz transparent layer gradually increases from 15 (FG196–1) to 25 (FG196–5) meters; seismic reflection transparent layer less than 30 m thick. Manganese nodules from FG196–3 are round-shaped, coated with brown soil-like film.
Brown to dark brown clay	IDPs, DPs	6.4	—	
Brown to dark brown clay	D	12.1	30	
Brown to dark brown sil. fossil-rich clay	IDs+r, DPs+r	27.6	50	
Brown to dark brown clay	DPs	20.1	70	

**Bottom sediment: Lithology was determined by microscopic observation of smear slide.

***Topography and others are described for each station area.

St. no.	Observ. no.	Date		Recalculated position			Corrected depth (m)
		Julian	Local	Latitude	Longitude	E.E.	
1595	FG197-1(c)	23	23	9°46.68′N	176°59.02′W	0.11	6298
	FG197-2(c)			9°45.93′N	176°58.33′W	0.13	6293
	FG197-3			9°45.19′N	176°57.68′W	0.16	5855
	FG197-4(c)			9°44.44′N	176°56.98′W	0.19	5848
1596	FG198-1(c)	24	23	8°57.56′N	176°23.96′W	0.17	6009
	FG198-2(c)			8°56.76′N	176°23.44′W	0.19	6129
	FG198-3(c)			8°55.96′N	176°22.94′W	0.22	6120
	FG198-4(c)			8°55.14′N	176°22.43′W	0.24	6063
1597	FG199-1(c)	24	24	7°38.13′N	175°14.54′W	0.26	5945
	FG199-2			7°38.21′N	175°14.43′W	0.25	5936
1598	B4	25	24	6°49.67′N	174°47.63′W	0.17	5962
	FG200-1(c)			6°49.74′N	174°47.95′W	0.21	5961
	FG200-2(c)			6°49.78′N	174°47.86′W	0.20	5954
1599	FG201-1(c)	25	25	5°29.19′N	173°47.67′W	0.31	4901
	FG201-2(c)			5°28.35′N	173°47.06′W	0.28	5179
	FG201-3			5°27.52′N	173°46.44′W	0.25	5245
	FG201-4			5°26.66′N	173°45.82′W	0.22	5277
	FG201-5(c)			5°25.83′N	173°45.17′W	0.19	5284
1600	B5	26	25	4°41.39′N	173°11.89′W	0.15	5584
	FG202-1(c)			4°41.39′N	173°12.50′W	0.16	5590
	FG202-2(c)			4°41.42′N	173°12.31′W	0.15	5586
1601	B6	26	26	3°17.83′N	172°10.51′W	0.33	5350
	FG203-1(c)			3°17.45′N	172°10.38′W	0.25	5349
	FG203-2(c)			3°17.24′N	172°10.34′W	0.26	5335

(Continued)

Bottom sediment	Manganese nodules			Topography and others
	Morphology	Abun. (kg/m²)	Cover. (%)	
Dark yellowish brown sil. fossil-rich clay	IDPs+r, DPs+r	31.7	40	Rough in abyssal knoll area; 3.5 kHz transparent layer poorly developed; seismic reflection transparent layer is hardly recognizable.
Dark yellowish brown clay	IDPs, DPs	22.4	50	
Dark yellowish brown clay	IDPs	11.9	—	
No sample	IDPr	(0.5)	(40)	
Dark brown sil. fossil-rich clay	IDPs	(1.9)	(10)	Rolled; seismic transparent layer is indistinct on the record.
Dark brown sil. fossil-rich clay	IDPs+r	4.8	30	
Dark brown sil. fossil-rich clay	IDPs	21.0	40	
Dark brown sil. fossil-rich clay	IDPs	19.6	40	
Dark yellowish brown sil. fossil-rich clay	SPr, Sr	0.7	10	Smooth; 3.5 kHz transparent layer several to 18 meters thick; seismic transparent layer is indistinct; western marginal part of the turbidite area according to the GH78–1 cruise report.
Dark yellowish brown sil. fossil -rich clay	SPr, Sr	5.0	—	
Dark brown sil. fossil-rich clay	Sr	tr	—	Abyssal plain area; very smooth; 3.5 kHz transparent layer 22 m thick; seismic reflection record shows that a transparent layer overlies turbidites (ca. 70 m thick collectively).
Dark brown sil. fossil-rich clay	Sr	0.1	0	
Dark brown sil. fossil-rich clay	Sr	tr	0	
No sample	No sample	0	(5)	Steeply (FG201–1) to gently (FG 201–2 to –5) sloped on the southern flank of a seamount; seismic reflection transparent layer indistinct.
Brown to dark brown calcareous marly ooze	Sr	1.0	0	
Dark brown silic.? calc. marly ooze	Sr	0.2	—	
Dark brown calcareous mud	Sr, SPr	tr	—	
Very dark greyish brown silic.-calc. mud	Sr	tr	0	
Dark brown silic. mud	No sample	0	—	Rolled; 3.5 kHz transparent layer 75 m+ thick; seismic reflection transparent 200 m or more thick, with interbedded distinct reflectors.
Dark brown silic. mud	No sample	0	0	
Dark brown silic. mud	Sr	tr	0	
Dark yellowish brown Silic. mud	Sr	1.2	—	Rolled; 3.5 kHz transparent layer and seismic reflection transparent layer about 100 m thick. Sampling sites are on the depression area surrounded by high abyssal knolls.
Dark yellowish brown Silic. mud	Sr	2.6	1	
Dark yellowish brown Silic. mud	Sr	8.3	1	

Appendix I-2

St. no.	Observ. no.	Date		Recalculated position			Corrected depth (m)
		Julian	Local	Latitude	Longitude	E.E.	
1602	B7	27	26	2°33.26′N	171°37.69′W	0.23	5389
	FG204–1(c)			2°33.39′N	171°37.33′W	0.19	5386
	FG204–2(c)			2°33.30′N	171°37.27′W	0.18	5386
1603	P159(H15)	27	27	1°17.22′N	170°42.28′W	0.16	5479
	FG205–1(c)			1°17.60′N	170°42.01′W	0.17	5511
	FG205–2(c)			1°17.46′N	170°42.05′W	0.16	5509
1604	B8	28	27	0°24.23′N	170°02.51′W	0.12	5457
	FG206–1(c)			0°24.82′N	170°02.74′W	0.12	5459
	FG206–2(c)			0°24.74′N	170°02.71′W	0.12	5457
1605	P160(H16)	28	28	0°57.91′S	169°01.69′W	0.16	5455
	FG207–1(c)			0°57.38′S	169°01.45′W	0.13	5459
	FG207–2(c)			0°57.47′S	169°01.40′W	0.12	5452
1606	B9(c)	29	28	1°45.07′S	168°26.20′W	0.19	5230
	FG208–1(c)			1°44.84′S	168°25.86′W	0.25	5215
	FG208–2(c)			1°44.92′S	168°25.79′W	0.25	5215
1607	P161(H17)	29	29	3°02.12′S	167°29.91′W	0.13	5698
	FG209–1(c)			3°02.21′S	167°29.09′W	0.32	5690
	FG209–2(c)			3°02.13′S	167°29.16′W	0.31	5692

(Continued)

Bottom sediment	Manganese nodules			Topography and others
	Morphology	Abun. (kg/m^2)	Cover. (%)	
Dark yellowish brown silic. mud	No sample	0	—	Slightly rolled; 3.5 kHz transparent layer 75 m thick; seismic reflection transparent layer about 150 m thick, interbedded with a continuous reflector in the middle part.
Dark yellowish brown silic. mud	No sample	0	0	
Dark yellowish brown silic. mud	No sample	0	0	
Dark brown silic. mud	No sample	0	—	Slightly rolled; 3.5 kHz transparent layer 75 m+thick; seismic transparent layer 90 m thick. P159 (7.09 m long) consists of silic. mud (0 to 1.5 m) and silic ooze (1.5 to 7.09 m).
Dark brown silic. mud	Sr	tr	0	
Dark brown silic. mud	Sr, SPr	0.3	0	
Dark yellowish brown silic. mud	No sample	0	—	Slightly rolled, with abyssal knolls up to 250 high. Sampling sites are on the top of a knoll with a height of 250 m; not underlain by 3.5 kHz transparent layer; seismic reflection transparent layer is indistinct, due to diffractions.
Dark yellowish brown silic. mud	No sample	0	0	
Dark yellowish brown silic. mud	Sr	0.1	0	
Dark brown $CaCO_3$-rich silic. mud	No sample	0	—	Flat at the southern foot of a small seamount; 3.5 kHz transparent layer thick; seismic transparent layer about 110 m thick. P160 (8.24 m long) consists of dark brown silic. mud, silic.-calc. mud, or $CaCO_3$-rich silic. mud (0 to 0.62 m) and silic. mud (0.62 m to 8.24 m).
Dark brown $CaCO_3$-rich silic. mud	No sample	0	0	
Dark brown $CaCO_3$-rich silic. mud	No sample	0	0	
Dark brown silic. mud	DPs	(57)	0	Southern lower slope of the southern ridge of the Nova-Canton Trough; 3.5 kHz transparent layer very thin; seismic reflection transparent layer not present.
Dark brown silic. calcareous ooze	No sample	0	5	
Dark brown silic. calcareous ooze	Sr, SEr	2.7	0	
Dark yellowish brown silic. mud	DPs, SPs	(7)	—	Rolled by abyssal knolls; 3.5 kHz transparent layer 7–8 m thick; no seismic reflection transparent layer. P161 (7.83 m long) consists of dark yellowish brown silic. mud (0 to 0.40 m), very dark brown pelagic clay and zeolitic mud (0.40 to 5.62 m), separated from very dark brown zeolitic mud (5.62 to 7.83 m) with a sharp boundary.
Dark yellowish brown silic. mud	IDPs	12.0	10	
Dark yellowish brown silic. mud	IDPs	11.6	30	

Appendix I-2

St. no.	Observ. no.	Date		Recalculated position			Corrected depth (m)
		Julian	Local	Latitude	Longitude	E.E.	
1608	B10	30	29	3°52.00′S	166°52.37′W	0.14	5618
	FG210–1(c)			3°51.98′S	166°51.92′W	0.32	5417
	FG210–2(c)			3°52.06′S	166°51.87′W	0.33	5434
1609	P162(H18)	30	30	5°11.60′S	165°51.90′W	0.20	4397
	FG211–1(c)			5°12.54′S	165°50.69′W	0.29	4395
	FG211–2			5°12.59′S	165°50.61′W	0.31	4395
1610	FG212–1(c)	31	30	6°00.76′S	165°21.53′W	0.15	2998
	FG212–2(c)			6°01.55′S	165°22.20′W	0.18	2602
	FG212–3(c)			6°02.36′S	165°22.85′W	0.21	2698
	FG212–4(c)			6°03.19′S	165°23.52′W	0.24	2740
1611	B11	31	31	7°20.88′S	164°17.60′W	0.16	4155
	FG213–1(c)			7°20.47′S	164°17.41′W	0.13	4156
	FG213–2(c)			7°20.58′S	164°17.40′W	0.14	4154
1612	P163(H19)	32	31	8°01.08′S	163°48.40′W	0.31	4808
	FG214–1(c)			8°01.20′S	163°47.88′W	0.4	4805
	FG214–2(c)			8°01.30′S	163°47.84′W	0.41	4805
			February				
1613	B12	32	1	9°29.32′S	162°41.40′W	0.17	2944
	FG215–1			9°29.08′S	162°41.35′W	0.17	2952
	FG215–2(c)			9°29.21′S	162°41.36′W	0.17	2945

(Continued)

Bottom sediment	Manganese nodules			Topography and others
	Morphology	Abun. (kg/m²)	Cover. (%)	
White to very pale brown nanno-foram ooze	(DPs)	tr	—	Rolled by abyssal knolls; 3.5 kHz transparent layer 0 to 35 meters thick; seismic reflection layer varies in thickness; the sampling sites are on the top to upper slope area of a small knoll.
Dark yellowish brown silic. mud	(DPs)	tr	(10)	
White nanno-foram ooze	(DPs)	tr	(10)	
	(DPs)	tr	—	Lower slope of the Manihiki western Plateau; 3.5 kHz transparent layer locally thinly developed; seismic reflection record shows reflective layers of younger age; FG sites lack the 3.5 kHz transparent layer. P162 (penetration: 7.50 m) consists of nanno-foram and foram-nanno ooze, partly clayey and including pebble to granule clasts.
Pale brown clayey nanno-foram ooze	DPs	tr	2	
No sample	DPs, IDPs	1.2	—	
No sample	No sample	0	0	Very rough; without transparent layer of 3.5 kHz and seismic reflection records.
No sample	No sample	0	0	
No sample	No sample	0	0	
No sample	No sample	0	0	
Light yellowish brown clayey nanno ooze	Vs	0.8	—	Rolled; 3.5 kHz record shows a transparent layer of 50 m thick with turbidite-like fine reflections.
Light yellowish brown clayey foram-rich nanno ooze	Vs	0.1	5	
Light yellowish brown clayey foram-rich nanno ooze	No sample	0	2	
Dark reddish brown calcareous mud	No sample	0	—	Flat; interbedded sequence of opaque and semi-transparent layers on 3.5 kHz record, 110 m thick, underlain by a sequence of weak reflections. P163 (7.87 m long) consists of dark reddish brown calc. mud (0 to 0.94 m) underlain by very pale brown clayey nanno ooze (partly foraminifera rich) (0.94 to 7.87 m), located within the Danger Island Trough.
Dark reddish brown nanno mud	No sample	0	0	
Dark reddish brown nanno mud	(Sr)	tr	0	
Very pale brown foram ooze	No sample	0	0	Flat, semi-opaque layer on 3.5 kHz record is developed, finely interbedded with semi-transparent layer; on seismic reflection record layered structure with weak reflections of 230 m thick is developed.
Very pale brown clayey nanno-foram ooze	No sample	0	—	
No sample	No sample	0	0	

St. no.	Observ. no.	Date		Recalculated position			Corrected depth (m)
		Julian	Local	Latitude	Longitude	E.E.	
1614	B13(c)	33	1	10°16.67′S	162°04.76′W	0.18	2763
	FG216–1(c)			10°16.18′S	162°05.17′W	0.14	2763
	FG216–2(c)			10°16.27′S	162°05.10′W	0.14	2764
1615	P164(H20)	33	2	11°36.55′S	161°05.41′W	0.20	3153
	FG217–1(c)			11°36.35′S	161°05.12′W	0.12	3155
	FG217–2(c)			11°36.30′S	161°05.16′W	0.13	3156
1616	B14	34	2	12°20.07′S	160°30.89′W	0.15	5690
	FG218–1(c)			12°20.54′S	160°31.28′W	0.30	5648
	FG218–2(c)			12°20.46′S	160°31.27′W	0.30	5637
1617	B15(c)	34	3	13°47.40′S	159°28.35′W	0.41	5162
	FG219–1(c)			13°47.03′S	159°28.25′W	0.17	5148
	FG219–2(c)			13°47.15′S	159°28.26′W	0.18	5147
1618	B16(c)	35	3	14°29.61′S	158°52.98′W	0.21	5453
	FG220–1(c)			14°29.76′S	158°53.12′W	0.17	5435
	FG220–2(c)			14°29.69′S	158°53.13′W	0.16	5438
—A	P165(H21)	35	4	14°28.86′S	158°52.66′W	0.21	5530
	FG221–1(c)			14°29.49′S	158°52.59′W	0.21	5484
	FG221–2(c)			14°29.37′S	158°52.53′W	0.22	5484
	FGV2			14°29.06′S	158°52.81′W	0.22	5495
1619	P166(H22)	46	15	13°34.03′S	157°06.01′W	0.17	5131
	FG222–1(c)			13°34.39′S	157°05.31′W	0.22	5110
	FG222–2(c)			13°34.28′S	157°05.42′W	0.22	5110
	B17(c)	47		13°34.29′S	157°05.16′W	0.21	5111

(Continued)

Bottom sediment	Manganese nodules			Topography and others
	Morphology	Abun. (kg/m²)	Cover. (%)	
Very pale brown clayey nanno-foram ooze	No sample	0	0	Flat; 3.5 kHz sequence is: semi-transparent layer, 12 m; semi-opaque layer with turbidite-like structure, 12 m; semi-opaque layer, 22 m; interbedded semi-opaque and semi-transparent layers, 112 m, in descending order.
No sample	No sample	0	0	
No sample	No sample	0	0	
Very pale brown clayey foram-nanno ooze	No sample	0	—	Western slope of the eastern ridge of the Manihi High Plateau; 3.5 kHz semi-opaque layer 120 m thick, underlain by opaque layer. P164 (6.11 m) consists of very pale brown foram-nanno ooze (0 to 2.12 m) and white nanno ooze (2.12 to 6.11 m).
No sample	No sample	0	0	
Very pale brown nanno-foram ooze	No sample	0	0	
Very dark brown pelagic clay	Ss, Ts, SPs	18.3	70	Flat at a sediment-filled narrow trough bottom; 3.5 kHz opaque layer interbedded with transparent thin layer; seismic reflection record shows strongly reflective layers without transparent layer.
No sample	No sample	0	60	
Very dark brown pelagic clay	Ss, DPs, Fs	8.6	50	
Very dark brown pelagic clay	Ss	31.0	60	Gently rolled; 3.5 kHz transparent to semi-opaque layer 30 m thick.
Very dark brown pelagic clay	Ss, DPs, IDPs	3.2	40	Seismic reflection transparent layer thinly developed.
Very dark brown pelagic clay	Ss	18.8	50	
Dark reddish brown pelagic clay	Ss, SPs, Is	1.0	2	Slightly rolled bottom of a shallow trough with a depression of approximate depth of 350 m; 3.5 kHz transparent layer 0–12 m thick; seismic reflection semi-transparent layer developed. P165 (7.29 m long) consists of dark reddish brown pelagic clay (0 to about 1.0 m) and reddish black zeolitic mud (1.0 to 7.29 m) interbedded with thin layer of micronodule mud.
Dark reddish brown pelagic clay	DPs, Is	tr	5	
Dark reddish brown pelagic clay	Ss, Is	0.5	2	
Dark reddish brown pelagic clay	No sample	0	—	
Dark reddish brown pelagic clay	Is, DPs, Ss	3.9	8	
Dark reddish brown pelagic clay	Is, DPs	2.8	10	
(unsuccessful)	No sample	0	—	
Very dark brown zeolitic mud	DPs, IDPs	(15)	—	Rolled; 3.5 kHz transparent layer present but subtle.
Very dark brown zeolitic mud	DPs, Ts+r	12.8	15	P166 (penetration about 8 m) consists of very dark brown zeolitic mud with a pelagic clay stiff interbed (5 cm thick) at a depth of several tens-of-decacentimeters; intensely disturbed by flown-in.
Very dark brown zeolitic mud	DPs, SPs, ISPs	9.4	20	
Very dark brown zeolitic mud	DPs, IDPs	6.1	20	

St. no.	Observ. no.	Date		Recalculated position			Corrected depth (m)
		Julian	Local	Latitude	Longitude	E.E.	
1620	B18(c)	47	16	12°26.44′S	157°57.20′W	0.11	5285
	FG223–1			12°26.09′S	157°57.15′W	0.15	5263
	FG223–2(c)			12°26.17′S	157°57.10′W	0.15	5265
1621	B19(c)	48	16	11°35.38′S	158°34.91′W	0.29	5312
	FG224–1(c)			11°35.57′S	158°34.72′W	0.35	5317
	FG224–2			11°35.47′S	158°34.78′W	0.36	5318
1622	P167(H23)	48	17	10°16.35′S	159°35.57′W	0.19	5235
	FG225–1(c)			10°16.03′S	159°35.45′W	0.24	5221
	FG225–2(c)			10°16.12′S	159°35.39′W	0.23	5237
1623	B20(c)	49	17	9°26.14′S	160°14.83′W	0.18	4561
	FG226–1(c)			9°25.72′S	160°14.68′W	0.22	4535
	FG226–2(c)			9°25.64′S	160°14.74′W	0.21	4539
1624	P168(H24)	49	18	8°08.05′S	161°12.37′W	0.20	3908
	FG227–1(c)			8°07.92′S	161°11.88′W	0.12	3889
	FG227–2(c)			8°07.84′S	161°11.92′W	0.12	3890
1625	B21(c)	50	18	7°06.72′S	161°56.68′W	0.15	4650
	FG228–1(c)			7°06.54′S	161°55.93′W	0.34	4648
	FG228–2(c)			7°06.47′S	161°55.98′W	0.34	4650

(Continued)

Bottom sediment	Manganese nodules			Topography and others
	Morphology	Abun. (kg/m^2)	Cover. (%)	
Dark reddish brown zeolitic mud	Ds	0.1	30	Rolled with abyssal knolls consisting of basement; 3.5 kHz transparent layer is 15 m thick with subtle lower boundary; seismic reflection pattern is strongly reflective (150 m thick).
Dark reddish brown zeolitic mud	Ss, SEs	23.9	40	
Dark reddish brown zeolitic mud	Ss, SEs	26.1	40	
Dark reddish brown zeolite-rich mud	Ds, Ss	6.7	40	Slightly rolled; 3.5 kHz transparent layer is less than 10 m to 13 m thick; seismic transparent layer is present.
No sample	Ss, Ds	3.8	30	
Dark reddish brown zeolite-rich mud	DPs, Ts	10.5	—	
Very dark brown zeolite-rich mud	No sample	0	—	Broadly rolled; 3.5 kHz transparent layer 17–18 m thick; seismic reflection transparent layer present. P167 (6.28 m long) consists of very dark brown zeolite-rich mud to zeolitic mud (0 to 0.83 m) and dark reddish brown zeolitic mud (0.83 to 6.28 m).
Dark reddish brown zeolite-rich mud	Ss, Ds	0.2	1	
Dark reddish brown zeolite-rich mud	Ss, SPs, Ds	0.2	1	
Brown to dark brown calcareous marly ooze	Ss, SPs	16.0	60	Northern foot of a small seamount, rough; 3.5 kHz transparent layer 7–8 m thick.
No sample	No sample	0	—	
No sample	No sample	0	—	
Very pale brown clayey nanno-foram ooze	No sample	0	—	Roughly rolled; 3.5 kHz transparent layer 12–13 m thick, gradually passing to underlying semi-transparent layer of 60 m+thick; both layers correspond to seismic transparent layer reflection underlain by strong reflections. P168 (5.70 m long) consists of clayey nanno-foram or foram-nanno ooze (0 to about 1.3 m) and nanno ooze (about 1.3 to 5.70 m).
Very pale brown clayey foram-nanno ooze	No sample	0	0	
Very pale brown clayey foram-nanno ooze	No sample	0	0	
Dark yellowish brown clayey nanno ooze	DPs, Ds	0.1	0	Flat at immediately north of a large seamount.
Dark yellowish brown clayey nanno ooze	Ss, Is	0.1	0	
Dark yellowish brown clayey nanno ooze	Ds, Is	tr	0	

Appendix I-2

St. no.	Observ. no.	Date		Recalculated position			Corrected depth (m)
		Julian	Local	Latitude	Longitude	E.E.	
1626	P169(H25)	50	19	5°47.32′S	162°55.92′W	0.17	4711
	FG229–1(c)			5°47.29′S	162°55.63′W	0.23	4706
	FG229–2(c)			5°47.22′S	162°55.66′W	0.22	4706
1627	B22(c)	51	19	5°27.32′S	163°46.01′W	0.23	4995
	FG230–1(c)			5°27.49′S	163°45.63′W	0.17	5001
	FG230–2(c)			5°27.42′S	163°45.71′W	0.16	4997
1628	P170(H26)	51	20	3°30.50′S	164°09.94′W	0.20	4947
	FG231–1(c)			3°30.61′S	164°09.45′W	0.13	4981
	FG231–2(c)			3°30.63′S	164°09.44′W	0.12	4981
1629	B23(c)	52	20	2°53.00′S	164°57.31′W	0.22	5261
	FG232–1(c)			2°52.99′S	164°56.56′W	0.20	5212
	FG232–2(c)			2°52.92′S	164°56.72′W	0.20	5211
1630	P171(H27)	52	21	1°30.45′S	165°52.52′W	0.16	5537
	FG233–1(c)			1°30.80′S	165°51.91′W	0.14	5483
	FG233–2(c)			1°30.69′S	165°51.84′W	0.14	5485

(Continued)

Bottom sediment	Manganese nodules			Topography and others
	Morphology	Abun. (kg/m²)	Cover. (%)	
Yellowish brown clayey nanno ooze	No sample	0	—	Flat at a foot of a seamount; 3.5 kHz transparent layer 18 m thick, underlain by semi-opaque layer of weak reflections.
Yellowish brown clayey nanno ooze	No sample	0	0	
No sample	No sample	0	0	P169 (5.67 m long) consists of very dark brown silic. mud and silic. fossil-rich calc. mud, interbedded with white foram ooze and very pale brown foram-nanno ooze or cal. marly ooze. The core includes four marked graded cycles.
Very dark brown silic. & calc. f.-rich mud	Sr	tr	0	Flat basin bottom, possibly filled with turbidites; 3.5 kHz record missing.
Dark reddish brown silic. & calc. f.-rich mud	No sample	0	0	
Dark reddish brown silic. & calc. f.-rich mud	No sample	0	0	
Dark yellowish brown silic. f. rich clayey nanno ooze	No sample	0	—	Rather rough in general, but flat at the sampling sites; transparent layer is little developed on 3.5 kHz and seismic reflection records.
Dark yellowish brown silic. f. rich clayey nanno ooze	No sample	0	0	
No sample	Ir	0.2	0	P170 (penetration about 4.3 m) represents a thin sediment cover on older lithified sequence; consists of dark yellowish brown silic. fossil rich nanno ooze (0 to 0.34 m), dark yellowish brown to dark brown silic. fossil-rich clay (0.34 to 2.0 m), dark brown pelagic clay (2.0 to 3.2 m), and very dark brown zeolite-micronodule-rich clay (3.2 to 3.83 m).
Dark yellowish brown siliceous mud	Ir, IDPr, Sr, Ts+r	6.1	0	Very rough as a whole; the sampling sites are in interknoll area; 3.5 kHz transparent layer 15 m thick. FG sediment samples represent lithology at a depth of about 15 cm below the sea floor.
Dark yellowish brown calc. f.-rich silic. mud	Sr, Ds·r, Ts+r	7.0	0	
Dark yellowish brown calc. f.-rich silic. mud	Sr, SEr	0.4	0	
Dark yellowish brown siliceous mud	No sample	0	—	Smooth; 3.5 kHz transparent layer 75 m+thick; seismic reflection transparent layer 70 m thick, underlain by turbidites of 110 m thick.
Dark brown siliceous mud	Sr	tr	0	
Dark brown siliceous mud	Sr	tr	0	P171 (7.85 m long) consists of dark yellowish brown sili. mud, associated with silic. fossil-rich clay and silic. ooze.

St. no.	Observ. no.	Date		Recalculated position			Corrected depth (m)
		Julian	Local	Latitude	Longitude	E.E.	
1631	B24(c)	53	21	0°58.61′S	166°20.89′W	0.14	5342
	FG234–1(c)			0°59.02′S	166°20.41′W	0.11	5390
	FG234–2(c)			0°58.94′S	166°20.49′W	0.10	5355
1632	P172(H28)	53	22	0°26.16′N	167°33.83′W	0.24	5255
	FG235–1			0°25.88′N	167°33.55′W	0.15	5240
	FG235–2(c)			0°25.99′N	167°33.63′W	0.16	5251
1633	B25(c)	54	22	1°16.04′N	168°09.97′W	0.22	5359
	FG236–1(c)			1°15.69′N	168°09.52′W	0.20	5367
	FG236–2(c)			1°15.82′N	168°09.56′W	0.19	5360
1634	P173(H29)	54	23	2°32.13′N	169°06.07′W	0.30	5087
	FG237–1(c)			2°31.48′N	169°05.67′W	—	5082
	FG237–2(c)			2°31.51′N	169°05.59′W	—	5060
1635	B26	55	23	3°16.42′N	169°40.10′W	0.14	5351
	FG238–1(c)			3°16.46′N	169°40.22′W	0.21	5374
	FG238–2(c)			3°16.35′N	169°40.22′W	0.22	5352
—A	FG239–1(c)	55	24	3°16.29′N	169°41.35′W	0.21	5349
	FG239–2(c)			3°16.30′N	169°41.29′W	0.20	5358
	P174(H30)			3°16.31′N	169°40.25′W	0.23	5350
	D377			3°16.08′N ~ 3°16.16′N	169°39.41′W ~ 169°41.15′W	0.17 ~ 0.40	5396 ~ 5373

(Continued)

Bottom sediment	Manganese nodules			Topography and others
	Morphology	Abun. (kg/m^2)	Cover. (%)	
Dark yellowish brown calc. silic. ooze	Sr	2.5	0	Slightly rolled; 3.5 kHz transparent layer 75 m+thick; seismic reflection transparent layer 140 m thick, associated with weak reflections in the lower part.
Dark yellowish brown calc. silic. ooze	SPs·r, Ss·r	9.0	0	
Dark yellowish brown calc. silic. ooze	SPs·r, Ss·r	10.4	5	
Brown to dark brown siliceous nanno mud	No sample	0	—	Rolled by repeated abyssal knolls and basins. The sampling sites are on the topographic high, standing about 200 m on basin floor; seismic reflection transparent layers 150 m. P172 (7.62 m long) consists of dark brown silic. ooze, except for the intervals 0 to 7 cm (silic. nanno mud), 27 to 46 cm and 85 to 94 cm (silic. fossil rich nanno ooze).
Dark yellowish brown calcareous siliceous mud	No sample	0	0	
Dark yellowish brown calcareous siliceous mud	Sr	tr	1	
Dark yellowish brown siliceous ooze	No sample	0	0	Very rough by repeated abyssal knolls. The sampling sites are at a foot of abyssal knoll. FG sediment samples represent lithology at a depth of about 15 cm below the sea floor.
Dark yellowish brown calc. siliceous ooze	No sample	0	0	
Dark yellowish brown calc. siliceous ooze	No sample	0	0	
Brown silic. calc. marly ooze	Dr	(6)	—	slightly rolled at a foot of seamount; 3.5 kHz and seismic reflection transparent layer 35 to 40 m each. P173 (7.99 m long) consists of silic. ooze, except for the top 55 cm thick part (silic. calc. marly ooze) and the lower part (6.7 to 7.99 m; silic. nanno ooze).
Brown to dark brown siliceous ooze	IDPs·r, DPs·r	6.8	5	
Brown to dark brown siliceous ooze	IDPs·r, DPs·r	7.7	10	
Brown to dark brown siliceous ooze	Sr, Dr	2.6	0	Rolled by abyssal knolls and basins. The sampling sites are on the slope and the top areas of an abyssal knoll standing about 300 m from basin floor. The sites are underlain by 3.5 kHz transparent layer of 45 to 50 m thick and by seismic reflection transparent layer of ca. 70 m thick. Located on the same abyssal knoll; seismic transparent layer is little developed. P174 (7.89 m long) consist exclusively of yellowish brown to dark yellowish brown silic. ooze, intensely bioturbated by rind burrows, chondrites, Zoophycos, etc.
Brown to dark brown siliceous ooze	Sr, Dr	5.0	5	
Brown to dark brown siliceous ooze	Sr, Dr	2.0	0	
Brown to dark brown siliceous ooze	IDPs·r, DPs·r, Ts·r	5.9	15	
Brown to dark brown calc. f.-rich silic. ooze	IDPr, Dr	1.2	0	
Dark yellowish brown siliceous ooze	No sample	0	—	
No sample	Ir, Vr, Sr	—	—	

St. no.	Observ. no.	Date		Recalculated position			Corrected depth (m)
		Julian	Local	Latitude	Longitude	E.E.	
1636	P175(H31)	56	25	4°43.37′N	170°42.88′W	0.1	5747
	FG240–1(c)			4°43.04′N	170°42.40′W	0.39	5736
	FG240–2(c)			4°43.08′N	170°42.32′W	0.42	5743
1637	B27(c)	57	25	5°31.51′N	171°18.84′W	0.11	5970
	FG241–1(c)			5°31.36′N	171°18.67′W	0.30	5972
	FG241–2(c)			5°31.44′N	171°18.74′W	0.33	5970
1638	P176(H32)	57	26	6°48.65′N	172°15.46′W	0.26	5791
	FG242–1(c)			6°48.95′N	172°15.53′W	0.19	5836
	FG242–2(c)			6°48.86′N	172°15.44′W	0.18	5839
1639	B28	58	26	7°40.26′N	172°56.77′W	0.22	5926
	FG243–1(c)			7°40.17′N	172°56.35′W	0.14	5907
	FG243–2(c)			7°40.28′N	172°56.45′W	0.15	5913
1640	P177(H33)	58	27	8°57.86′N	173°53.91′W	0.15	5915
	FG244–1(c)			8°58.05′N	173°53.34′W	0.11	5901
	FG244–2(c)			8°57.96′N	173°53.24′W	0.11	5902
1641	B29(c)	59	27	9°46.81′N	174°31.04′W	0.12	5829
	FG245–1(c)			9°46.78′N	174°30.71′W	0.17	5834
	FG245–2(c)			9°46.92′N	174°30.77′W	0.17	5839

(Continued)

Bottom sediment	Manganese nodules			Topography and others
	Morphology	Abun. (kg/m²)	Cover. (%)	
Dark brown siliceous mud	No sample	0	—	Slightly rolled; 3.5 kHz transparent layer 75 m+thick; seismic reflection transparent layer varies from 150 to 200 m in thickness, with a very weak reflection in the middle part. P175 (7.86 m long) consists of dark brown silic. mud throughout.
Brown to dark brown siliceous mud	Vr	tr	2	
Brown to dark brown siliceous mud	No sample	0	0	
Dark brown siliceous mud	No sample	0	0	Gently rolled; 3.5 kHz transparent layer 75 m+thick; seismic reflection transparent layer 150 m thick, underlain by reflective layer. Both the seismic layers are eroded at the trough south of the sampling sites.
Dark brown siliceous mud	No sample	0	0	
Dark brown siliceous mud	No sample	0	0	
Dark brown siliceous mud	No sample	0	—	Slightly rolled; 3.5 kHz and seismic reflection transparent layers about 100 m thick. P176 (7.84 m long) consists of dark brown silic. mud (0 to 0.05 m), dark brown to very dark greyish brown pelagic clay (0.05 to 1.6 m), very dark grayish brown silic. fossil-rich clay (1.6 to 3.65 m), dark brown bioturbated silic ooze (3.65 to 7.62 m), and dark brown silic. mud (7.62 to 7.84 m).
Brown to dark brown siliceous mud	Sr, Dr	0.4	0	
Brown to dark brown siliceous mud	Ir, Vr, SPr	0.1	0	
Dark brown siliceous mud	Vr, Sr	0.1	—	Rolled by abyssal knolls. The sites are on an abyssal knoll, underlain by 3.5 kHz transparent layer of 90 m thick and seismic reflection transparent layer of 100 m thick.
Dark brown silic.-f.-rich clay	Dr, Sr	0.2	0	
Dark brown silic.-f.-rich clay	Sr, Vr	0.6	0	
Dark brown siliceous mud	Dr	(2)	—	Slightly rolled at the north of the Magellan Trough; 3.5 kHz transparent layer 15 m thick; seismic reflection semi-transparent layer less than 20 m thick. P177 (7.87 m long) largely consists of dark brown pelagic clay, except for the top 40 cm part (silic. mud).
Dark brown siliceous mud	Sr, Ts+r	3.7	5	
Dark brown siliceous mud	Sr, SEr, SPr	10.0	15	
Dark brown silic.-f.-rich clay	Sr, SPr, Dr	7.8	30	Slightly rolled; 3.5 kHz transparent layer 25 m thick; seismic reflection transparent layer 30–40 m thick. FG sediment sample represents lithology at a depth of 15 to 20 cm below the sea floor.
No sample	Sr, SEr	1.8	30	
Dark brown pelagic clay	Sr, SEr	9.4	20	

St. no.	Observ. no.	Date		Recalculated position			Corrected depth (m)
		Julian	Local	Latitude	Longitude	E.E.	
1642	P178(H34)	59	28	11°06.38′N	175°30.07′W	0.13	5441
	FG246–1(c)			11°06.26′N	175°29.50′W	0.30	5430
	FG246–2(c)			11°06.19′N	175°29.45′W	0.29	5429
1643	D378	60	28	11°49.41′N～11°49.74′N	176°05.47′W～176°06.26′W	0.22～0.14	5258～5257
	FG247–1(c)			11°49.40′N	176°04.87′W	0.13	5253
	FG247–2(c)			11°49.36′W	176°04.84′W	0.12	5256
1644	P179(H35)	60	29	13°16.99′N	177°08.35′W	0.15	5027
	FG248–1(c)			13°16.75′N	177°08.19′W	0.23	5025
	FG248–2(c)			13°16.85′N	177°08.23′W	0.24	5027
1645	B30(c)	61	29	14°06.61′N	177°47.28′W	0.12	5068
	FG249–1(c)			14°06.20′N	177°46.83′W	0.16	5123
	FG249–2(c)			14°06.30′N	177°46.88′W	0.15	5117
1646	B31(c)	61	March 1	15°22.48′N	178°45.46′W	0.11	5537
	FG250–1(c)			15°22.79′N	178°45.21′W	0.31	5512
	FG250–2(c)			15°22.74′N	178°45.17′W	0.32	5526
1647	B32(c)	62	1	16°10.14′N	179°19.82′W	0.21	5292
	FG251–1(c)			16°10.17′N	179°19.87′W	0.21	5292
	FG251–2(c)			16°10.10′N	179°19.81′W	0.20	5291

(Continued)

Bottom sediment	Manganese nodules			Topography and others
	Morphology	Abun. (kg/m²)	Cover. (%)	
Brown to dark brown silic.-f.-rich clay	Ds	(1)	—	Very slightly rolled; 3.5 kHz transparent layer 10 to 11 m thick; seismic reflection transparent layer is difficult to be discriminated.
Brown to dark brown silic.-f.-rich clay	DPs, IDPs	27.2	80	
Brown to dark brown silic.-f.-rich clay	DPs, IDPs	22.4	70	P178 (7.82 m long) consists of thin layer of brown to dark brown silic. fossil-rich clay (at the top), dark brown pelagic clay (~4.60 m), brown zeolite rich clay (4.60 to 7.00 m), and dark reddish brown zeolitic mud (7.00 to 7.82 m).
No sample	DPs, IDPs	—	—	Southeastern lower slope of a small rise, centered at 12°10′N, 177°25′W.
Dark brown zeolite-rich clay	DPs, IDPs	9.8	70	3.5 kHz transparent layer 15 to 20 m thick; seismic reflection transparent layer very thinly developed.
Dark brown zeolite-rich clay	DPs, IDPs	21.8	70	
Dark brown zeolitic mud	No sample	0	—	Smooth at a northern foot of a seamount; 3.5 kHz semi-transparent layer 9 m (FG sites) to 5 m (P site) in thickness; seismic reflection transparent layer can not be distinguished. P179 (3.37 m long) represents the entire sedimentary sequense overlying hard rocks; consists of dark brown to dark reddish brown zeolitic mud (0 to 2.3 m), dark reddish brown thin-bedded zeolitic mud with altered volcanic ash layer, including slump-folds (2.3 to 3.28 m), and dark yellowish brown hard siltstone and chert (3.28 to 3.37 m).
Dark brown zeolitic mud	No sample	0	10	
No sample	SPs+r	0.2	8	
Dark brown zeolite-rich clay	Ds, DPs	20.2	80	Rather rough at northern foot of a large knoll. 3.5 kHz transparent layer 12 m thick; seismic reflection transparent layer is not present.
Dark brown zeolite-rich clay	DPs, IDPs, Es	23.4	80	
Dark brown zeolite-rich clay	DPs, IDPs	21.8	80	
Dark brown zeolite-rich clay	Ds, DPs, Ts	2.1	30	Smooth at abyssal basin; 3.5 kHz transparent layer 13 m thick. FG sediment samples represent lithology at a depth of 15 cm below the sea floor.
Dark brown zeolitic mud	Ts, Ds	7.2	40	
Dark brown zeolitic mud	DPs, Ts	5.5	30	
Dark brown zeolitic mud	Ds	15.4	80	Flat at inter-knoll basin, underlain by 3.5 kHz transparent layer of 45 to 50 m thick.
Dark brown zeolitic mud	Fs	6.2	50	
Dark brown zeolitic mud	Ds, Ss	13.5	70	